

# Performances of the phasing sensors for the M4 adaptive unit

Runa Briguglio<sup>a</sup>, Giorgio Pariani<sup>b</sup>, Marco Xompero<sup>a</sup>, Armando Riccardi<sup>a</sup>, Matteo Tintori<sup>b</sup>,  
Elise Vernet<sup>c</sup>, and Marc Cayrel<sup>c</sup>

<sup>a</sup>INAF Osservatorio Astrofisico Arcetri L. E. Fermi 5, 50125 Firenze Italy

<sup>b</sup>ADS-International, Via Pio Galli - sindacalista 3, 23841 Annone di Brianza Lecco, Italy

<sup>c</sup>ESO, Karl-Schwarzschild-Str. 2, 85748 Garching bei Munchen, Germany

## ABSTRACT

We report the integration, verification and performances of the absolute phase sensors for the co-phasing of the ELT adaptive M4 mirror. The phase sensors (named as Sensors of Phase Lag, SPL) are composed by a tunable, narrow-band source and an optical head to illuminate a 10 mm diameter area across two mirror segments. Their absolute vertical distance is computed by comparing the PSF profiles obtained at different wavelengths. The laboratory verification showed that the sensor accuracy is 10 nm at 0 differential phase and better than 80 nm in the full capture range of -10 to 10  $\mu\text{m}$ . In the paper we will describe the sensors integration, the optical test bench and we will discuss the performances in the frame of the optical calibration of the M4 adaptive mirror.

**Keywords:** Adaptive Optics, Wavefront correctors, Phase sensors, Optical calibration, Laser Interferometry

## 1. CO-PHASING OF THE ELT ADAPTIVE MIRROR M4

The M4 adaptive mirror, which is currently under manufacturing, will be the wavefront corrector for E-ELT, serving all its focal station. The mirror technology has been adapted from that of the LBT and VLT adaptive secondary mirrors (see e.g.<sup>1</sup>).

The mirror is controlled by 5316 voice coil actuators and is segmented into six petals so that the co-phasing of the optical surface is requested to allow high contrast and high resolution imaging.

The optical characterization and calibration of the M4 unit is derived from the procedure for large format deformable mirrors (see e.g.,<sup>23</sup>) and included the co-phasing, will be performed on a dedicated Optical Test Tower (OTT) with the feedback of a He-Ne interferometer. A first demonstration of the co-phasing has been performed on the demonstration prototype.<sup>4</sup> Due to its intrinsic phase ambiguity, the interferometer is however sensitive to the differential WF piston amongst the shells modulo  $\lambda/2$  only. An additional device is then requested to solve the phase ambiguity and to perform the segments co-phasing. The instrument designed to this purpose for the OTT, under the responsibility of INAF (Italian Institute for Astrophysics) is the Sensor of Phase Lag (SPL). Since the SPL is sensitive to the absolute phase, it is suitable to measure the *true* differential piston amongst neighbouring segments and correct the interferometer reading.

Within the co-phasing procedure of the M4 unit, the SPL measurements will be started after the individual flattening of the segments and the correction of the local (differential) alignment amongst them.<sup>5</sup> The SPL readings will be used as a reference to correct the piston signal ambiguity as retrieved by the interferometer; the corrected phase-map will then be used to co-phase the segments. The procedure will be iterated to check the proper correction of differential alignment (segments tip/tilt) and piston.

---

Further author information:

Runa Briguglio: E-mail: runa@arcetri.astro.it, Telephone: +39 055 2752200

## 2. THE SENSOR OF PHASE LAG

The concept of the SPL and its design are extensively described in the literature:<sup>6</sup> it consists basically in an illuminator to shine a collimated beam across the segments gap; the reflected light is focused onto a CCD to image the PSF produced by the illuminated area. The source is narrow band and tunable in wavelength; the comparison of the PSF obtained at different colors yields the information of the differential piston. In particular, when the shape of the PSF does not change for the different colors, the differential piston is expected to be null within the sensitivity of the device. A more detailed description of the working principle, including the measurement simulation, is given in the following.

A single SPL measurement is composed by the 6 values read by the separate units. In order to complete a measurement a set of frames are collected from the high resolution camera installed on the units, each frame being associated to a given band-pass as set on the tunable filter. The measurement flow is summarized as follows:

1. the tunable filter is set to a given wavelength  $\lambda_i$ ;
2. the proper exposure time for the selected wavelength is chosen from a look-up table;
3. a frame  $\omega_i$  is captured from each camera and bias and dark are subtracted;
4. the PSF center is found and a bounding box is extracted; the pixel are rebinned vertically to obtain an average profile  $\beta_i$ ;
5. the sequence is iterated for all the wavelengths requested;
6. for each SPL unit, all the profiles  $\beta_i$  are piled up according to wavelength to build a fringes map  $\gamma$ ;
7.  $\gamma$  is compared (via a correlation algorithm) to a database of synthetic fringes map at different wavelength to find the best match.

For a proper identification of the PSF center on the frame, a wavelength scan is performed before starting the measurement; all the frames are summed up to obtain a *broad-band* PSF and evaluate the center.

The comparison database is created with a numerical code initialized with the actual physical properties of the units, such as the F/#, pixel size, fiber core size. The wavelength span for the database is larger and more resolved than the measurement one, so that the synthetic fringes map for the correlation is assembled on-line with the wavelength span currently used. Since the database is created over a differential piston step of 5 nm only, the matching errors are small (here we are not considering the effect of measurement noise which is however negligible as we demonstrated in the lab). Such high precision comes from computational arguments only so that we considered a measurement error of 50 nm from the theory. Such error is well within the requested accuracy.

## 3. TEST SETUP AND PROCEDURE

After integrating the units, we arranged a laboratory set-up for the verification and individual characterization of SPLs. The goal of the laboratory activities is primarily to check them against the top-level requirement: the absolute phase accuracy shall be better than 100 nm. The laboratory set-up includes a zero-piston reference and a piston simulator. The former is a precision flat mirror with a black stripe glued on its surface to simulate the M4 gap: the differential piston between the two areas (simulating therefore the M4 segments) is zero by design so that the device may be used as a precision reference to verify the SPL reading at zero piston. The piston simulator is a more complicated setup and will be described below.

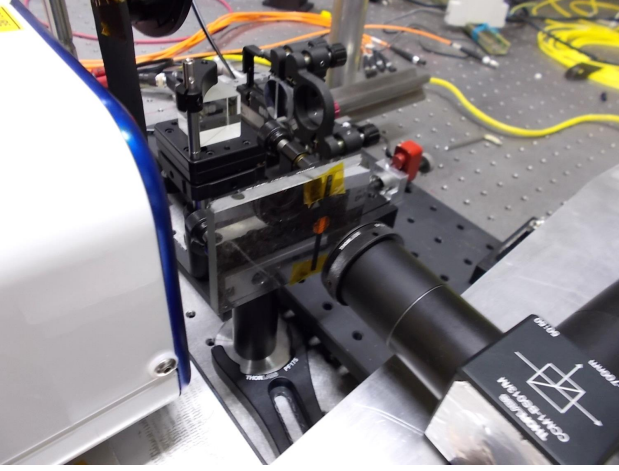


Figure 1. Test setup for the zero-piston measurement.

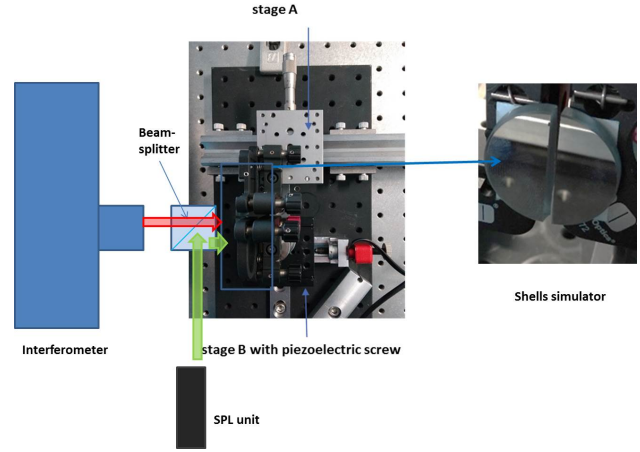


Figure 2. Schematic view of the SPL test bench, with the interferometer (on the left) to measure the shells simulator (on the right) as long as the shell is shifted with the piezo screw (red box in the central panel). The SPL units are installed on a separate bench and the measuring beam is folded by a beam splitter cube.

### 3.1 The piston simulator

The piston simulator setup is composed by 2 D-shaped mirrors (acting as the imaged area of two shells), a piezoelectric screw to shift one of the mirror (and produce a differential piston between them) and an interferometer as feedback for the applied differential piston (refer to Fig. 3). The mirror optics is obtained by cutting a flat protected aluminum mirror in halves (see Fig. 2). The two halves are glued on two stages A and B. Stage A provides fine motion in the direction perpendicular to the shell gap to set the correct shell distance, while stage B is driven by a piezoelectric screw to set the differential piston between the two shells. Both mirrors are equipped with tip/tilt stages to allow the removal of the differential tilt between the shells and the superposition of the two PSFs on the camera. A non-polarizing beam-splitter is used to allow monitoring the shell simulator by both the interferometer and SPL. The interferometer is on the transmission arm and the SPL on the reflection one. We adjusted the interferometer position so that the center of the beam is in between the two mirrors.

The shell simulator is monitored by the interferometer through a non-polarizing beam splitter in transmission. The interferometer lateral-vertical position is adjusted to match the measuring beam of the SPL: we installed a pinhole on the output flange of the interferometer to identify the center of the frame. The SPLs are mounted on a lateral bench and their beam is directed to the shell simulator with the beam splitter in reflection. The SPL position and tilt is adjusted to have the measuring spot balanced on both mirrors. A filter-wheel with black caps is installed in front of the interferometer to block the beam during the SPL measurement.

### 3.2 Verification of the piezo-electric actuator

The piezoelectric screw (Picomotor) is the key-elements in the procedure since it shall produce the piston-displacement for the SPL verification. Within this scope, the screw shall fulfill a single major requirement: it shall be capable of producing steps lower than the interferometer phase-ambiguity threshold (315 nm). The precision and repeatability of the commands are of lower importance, since the resulting displacement is monitored by the interferometer. The Picomotor has been verified in front of the interferometer, by applying a sequence of commands and measuring the differential piston produced. The minimum command (1 step) corresponds to a nominal displacement of approximately 25 nm (from datasheet); we always considered for our purposes a command of 4 steps (100 nm), which also fulfills the phase-ambiguity threshold requirement. The Picomotor curve calibrated against the interferometer is shown in Fig. 4, where we measured an average displacement slope of 24 nm/step. We verified that the repeatability error is much lower than the  $\lambda/2$  threshold.

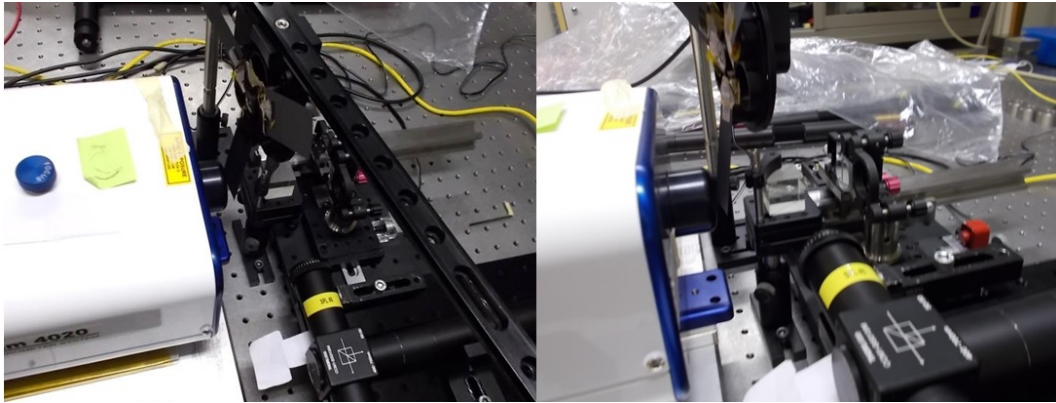


Figure 3. The SPL test bench after integration in the optical laboratory. For a description of the devices refer to Fig.2. The interferometer is the white box on the left and the SPL is the black "T" shaped assembly on the bottom. The rail (on the top) supports a filter-wheel with blocking mask to cut the interferometer laser during the SPL measurement.

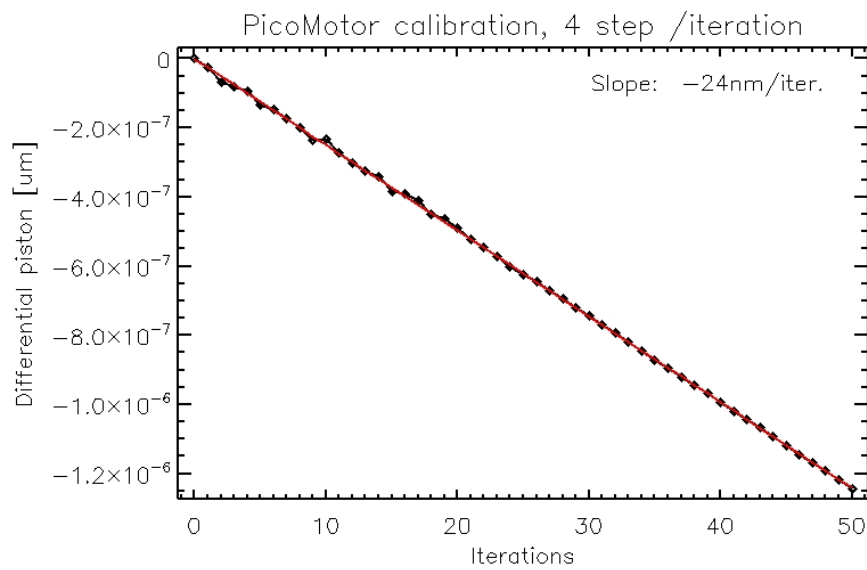


Figure 4. Verification of the piezo-electric actuator to produce a piston movement.

### 3.3 Wavefront calibration of the setup

The beam splitter used to monitor the shells simulator with the interferometer may introduce a differential piston signal. For instance, if the internal  $45^\circ$  surface has a curvature, the measurement will be affected by an astigmatism which in turn is seen as a differential tilt on the shell islands. When such a tilt is corrected with the TipTilt stages, a differential piston is added to the shells because of the off-axis pivot point of the mount. The size of the measuring spot (10 mm) is comparable to the pivot point off-axis so that we might expect a differential piston offset of the same amplitude of the residual tilt PtV. Such error affects differentially the reflection and transmission arms, i.e. the SPL and interferometer, and is a measurement offset between them. In order to assess this issue, we tested in reflection a set of beam-splitters and measured the differential tilt on the shell islands. We then adopted the one with the minimum differential tilt offset, provided it is lower than the SPL declared precision. After installation, we aligned the shell against the SPL, then measured the residual tilt on the transmission arm (interferometer) finding a maximum offset of 24 nm PtV (X) and 15 nm PtV (Y). The residue is shown in the picture below. During the alignment, we always considered the PSF of the individual shell as a reference for the alignment of the differential tilt.

### 3.4 Test procedure

The verification and validation procedure of the SPL units is composed by three test items. As first, we verify the zero reading with the zero-piston setup; then we perform a measurement run with the piston simulator, spanning a piston range of approximately  $-3 \mu\text{m}$  to  $+3 \mu\text{m}$  for 5 units and the broader range 500 nm to  $-10 \mu\text{m}$  for the sixth one. The final position reached by the piezo screw at the end of this piston run is absolutely calibrated thanks to the data processing (see below). With the piston simulator parked at this position, all the other SPL units are installed on the test bench and their readings are recorded, as the last test at the edge of the capture range. The interferometer keeps monitoring the shell simulator during the test to track any possible drifts.

The data analysis of the piston run is based on the comparison between the values measured by the interferometer and the SPL. We reconnect in phase the values read by the interferometer with the help of the SPL. To this purpose, we identify within the dataset the point where the SPL reading is the closest to zero. The SPL are successfully tested at zero piston, delivering a measurement precision lower than 10 nm (which is definitively lower than the phase ambiguity threshold, 315 nm). We may then rely on that measurement to adjust the interferometer reading by removing a phase offset which is an integer number of  $\lambda/2$ . Since the piezo screw steps are always shorter than 315 nm, the rest of the interferometer data points may be adjusted according to the same procedure.

## 4. RESULTS

### 4.1 Zero piston reading

The test consisted of a set of 20 consecutive measurements, captured in a time interval of approximately 30 minutes. For each sample of 20 values we evaluate mean, standard deviation and peak-to-valley. As mentioned, the synthetic fringe patterns are collected with a step of 5 nm, so that the scatter in the fit results is discrete as well. All SPL units showed an intrinsic accuracy lower than 5 nm and precision lower than 10 nm ptv. It is worth noting that the zero-piston setup has also zero differential tilt by design, so that any possible entanglement between local tilt and differential piston is solved. The beam alignment across the two simulated shells is checked within 1 mm approximately. We identify qualitatively a 10 nm/mm relation between beam off-center and piston error. Such value is to be compared to the sub-mm mounting accuracy in the OTT. The test results are shown in Tab.4.2.

### 4.2 Piston run test

The test consists in a number of simultaneous SPL and interferometer measurements, as long as the piezo screw shifts one shell in steps of approximately 100 nm. We phase-unwrap the interferometer values according to the procedure mentioned above, then we compute the linear fit of the SPL vs interferometer dataset and evaluate

SPL Id	Zero piston test			Full range test		
	Mean value	Stddev	PtV	Test range [nm]	Fit Slope	Fit offset [nm]
1	5 nm	2 nm	10 nm	-2340 to 3450	0.9925	14
2	0 nm	1 nm	5 nm	-3897 to 3079	0.9960	-42
3	3 nm	2 nm	5 nm	-3180 to 2740	0.9941	-27
4	0 nm	2 nm	5 nm	-2840 to 3380	0.9920	-29
5	0 nm	3 nm	10 nm	-3449 to 2810	0.9949	27
6	5 nm	0 nm	5 nm	-3347 to 2917	0.9929	46

Table 1. Results of the zero piston test and of the full range test.

SPL Id	SPL reading [nm]	Interf. reading [nm]	Diff. [nm]	Time since start [h]
1	10275	10274	1	0
2	10330	10315	15	0.45
4	10360	10362	-2	1.26
5	10435	10415	20	1.61
6	10420	10428	-8	1.99
3	10450	10452	-2	2.23

Table 2. SPL readings at full range, compared with the interferometer value.

the fit slope and offset and compute the residuals. The fit results are shown in table 4.2; the entire dataset is presented for the extended range run in Fig. 5

The fit offset (SPL value at zero interferometer reading) is due to the differential piston offset between the two measuring arms and it is however within specification. The fit slope is lower than 1 for all the SPL units: our guess is that such a differential reading comes from a projection effect in the two measuring arms; the point will be addressed in future laboratory activities.

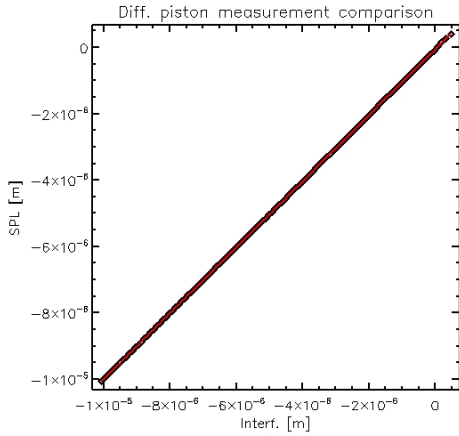


Figure 5. SPL readings vs interferometer during the extended range piston run. Red line: linear fit.

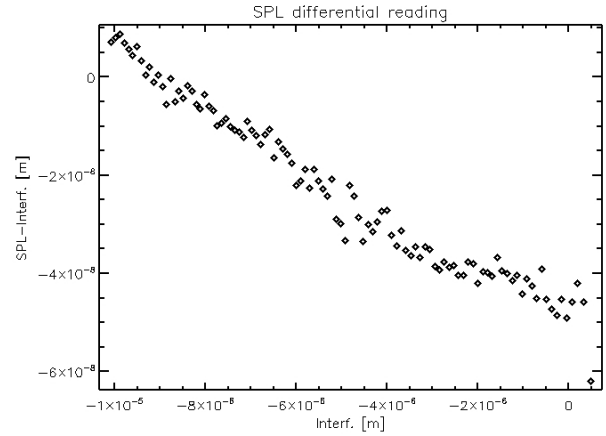


Figure 6. Difference between the SPL and interferometer piston run.

### 4.3 Piston reading at full range

The readings at full range (approximately 10  $\mu\text{m}$ ) for all the SPL units are shown below. As mentioned in the procedure, the measurement position are verified with the interferometer during the extended piston run. The individual measurements are also compared with the current interferometer reading. Data are arranged in chronological order to show that the scatter is likely due to a drift of the test bench. All the SPL units meet the REQ of 100 nm accuracy at 10  $\mu\text{m}$  offset.

## 5. DISCUSSION AND CONCLUSIONS

According to the laboratory experimentation, the SPL concept has been validated and the results meets very well the requirement. In particular, the zero-piston test, with the SPL units measuring a flat monolithic mirror divided into two regions by a black stripe, resulted in a typical 5nm PtV precision. The units were tested in the range (approximately) -3  $\mu\text{m}$  to 3  $\mu\text{m}$  and the measured accuracy is better than 50 nm: such accuracy may come however to a projection effect between the SPL and reference arm with the interferometer, to be further investigated. It is worth noting that, according to the M4 calibration procedure, the units were not expected to feature such very high precision; the precise measurement for the mirror phasing is foreseen to be based on the interferometer reading. The SPL serves as a calibrator for the interferometer measurements to solve the phase ambiguity. On the other side, such high precision will be very useful to speed up the phasing process in the OTT and also to help disentangling the local tip/tilt offset on the measurement area from the piston signal.

## REFERENCES

- [1] Biasi, R., Andrighettoni, M., Angerer, G., Mair, C., Pescoller, D., Lazzarini, P., Anaclerio, E., Mantegazza, M., Gallieni, D., Vernet, E., Arsenault, R., Madec, P. Y., Duhoux, P., Riccardi, A., Xompero, M., Briguglio, R., Manetti, M., and Morandini, M., “VLT deformable secondary mirror: integration and electromechanical tests results,” in [*Proc. of SPIE*], *Society of Photo-Optical Instrumentation Engineers (SPIE) Conference Series* **8447**, 84472G (Jul 2012).
- [2] Briguglio, R., Biasi, R., Xompero, M., Riccardi, A., Andrighettoni, M., Pescoller, D., Angerer, G., Gallieni, D., Vernet, E., Kolb, J., Arsenault, R., and Madec, P.-Y., “The deformable secondary mirror of VLT: final electro-mechanical and optical acceptance test results,” in [*Proc. of SPIE*], *Society of Photo-Optical Instrumentation Engineers (SPIE) Conference Series* **9148**, 914845 (Jul 2014).
- [3] Briguglio, R., Quirós-Pacheco, F., Males, J. R., Xompero, M., Riccardi, A., Close, L. M., Morzinski, K. M., Esposito, S., Pinna, E., Puglisi, A., Schatz, L., and Miller, K., “Optical calibration and performance of the adaptive secondary mirror at the Magellan telescope,” *Scientific Reports* **8**, 10835 (Jul 2018).
- [4] Briguglio, R., Xompero, M., Riccardi, A., and al., “Optical calibration of the M4 prototype toward the final unit,” in [*Proceedings of the Fourth AO4ELT Conference*], (Nov. 2015).
- [5] Briguglio, R., Pariani, G., Xompero, M., and al., “Optical calibration of the E-ELT adaptive mirror M4: testing protocol and assessment of the measurement accuracy,” in [*Proceedings of the Fifth AO4ELT Conference*], (July 2017).
- [6] Noethe, L. and Adorf, H. M., “Optical measurements of phase steps in segmented mirrors - fundamental precision limits,” *Journal of Modern Optics* **54**, 3–31 (Jan 2007).